Mon. Not. R. Astron. Soc. **000**, 000–000 (0000) Printed 26 January 2011 (MN LATEX style file v2.2)

Carbon Recombination Lines toward the Riegel-Crutcher Cloud and other Cold H I Regions in the inner Galaxy

D. Anish Roshi, [1⋆] & N. G. Kantharia, [2] †
[1] *National Radio Astronomy Observatory‡, Green Bank, WV 24944, USA*
Raman Research Institute, Bangalore, India 560 080 and
National Centre for Radio Astrophysics, Tata Institute of Fundamental Research, Pune, India.
[2] *National Centre for Radio Astrophysics, Tata Institute of Fundamental Research, Pune, India*

arXiv:1101.4901v1 [astro-ph.GA] 25 Jan 2011

26 January 2011

ABSTRACT

In the first paper in the series, Roshi, Kantharia & Anantharamaiah (2002) published the Galactic plane survey of carbon recombination lines (CRRL) at 327 MHz. CRRL were extensively detected from the inner Galaxy (longitudes$< 20^\circ$). We report here, for the first time, the association of low frequency CRRL with H I self-absorbing clouds in the inner Galaxy and that the CRRLs from the innermost $\sim 10^\circ$ of the Galaxy arise in the Riegel-Crutcher (R-C) cloud. The R-C cloud is amongst the most well known of H I self-absorbing (HISA) regions located at a distance of about 125 pc in the Galactic centre direction. Taking the R-C cloud as an example, we demonstrate that the physical properties of the HISA can be constrained by combining multi-frequency CRRL and H I observations. The derived physical properties of the HISA cloud are used to determine the cooling and heating rates. The dominant cooling process is emission of the C II 158 μm line whereas dominant heating process in the cloud interior is photoelectric emission. Constraints on the FUV flux (G0 $\sim$ 4 to 7) falling on the R-C cloud are obtained by assuming thermal balance between the dominant heating and cooling processes. The H_2 formation rate per unit volume in the cloud interior is $\sim 10^{-10} - 10^{-12}$ s^{-1} cm^{-3} , which far exceeds the H_2 dissociation rate per unit volume. We conclude that the self-absorbing cold H I gas in the R-C cloud may be in the process of converting to the molecular form. The cold H I gas observed as HISA features are ubiquitous in the inner Galaxy and form an important part of the ISM. Our analysis shows that combining CRRL and H I data can give important insight into the nature of these cold gas. We also estimate the integration times required to image the CRRL forming region with the upcoming SKA pathfinders. Imaging with the MWA telescope is feasible with reasonable observing times.

Key words: Galaxy: general — ISM: atom — ISM: general — ISM: structure — line:formation — radio lines:ISM

1 INTRODUCTION

In earlier papers (Roshi & Anantharamaiah 2000, 2001a, 2001b), we presented the details of a 327 MHz recombination line survey of the inner Galaxy made with the Ooty Radio Telescope (ORT). Results of the preliminary analysis of carbon recombination lines (CRRL) detected in this survey were presented in Roshi, Kantharia, Anantharamaiah (2002; Paper I). The CRRLs at low-frequencies ($\lesssim$ 1.4 GHz) arise in diffuse C II regions in the Galaxy. The ionisation potential of carbon (11.3 eV) is less than that of hydrogen (13.6 eV) and hence carbon can remain in the singly-ionised state outside regions where hydrogen is fully ionised. Low-frequency CRRLs are thus useful as diagnostics of partially ionised clouds. However, the reduced abundance of carbon (solar abundance relative to hydrogen 2.9×10^{-4}; Lodders 2003) and the consequent weak strength of the CRRLs makes the detection of these lines difficult. Generally stimulated emission or absorption against a strong background radiation field facilitate their detection.

The first CRRL from diffuse C II region was detected toward the direction of the supernova remnant Cas A and this

⋆ aroshi@nrao.edu
† ngk@ncra.tifr.res.in

direction has since been extensively observed in CRRL at frequencies ranging from 15 MHz in absorption to 1400 MHz in emission (Konovalenko & Sodin 1980, Blake Crutcher & Watson, 1980, Konovalenko 1984, 1990, Ershov et al. 1984, 1987, Payne, Anantharamaiah, Erickson 1989, Sorochenko & Walmsley 1991, Stepkin et al. 2007). Modelling showed that CRRLs originate in cool gas with $T_e \sim 35-75$K (Payne et al. 1994). The LSR velocity coincidence of the carbon lines with H I absorption observed toward Cas A and the similarity in the spatial distribution of the two lines across Cas A have led to the suggestion that the CRRL forming regions and H I absorption regions coexist (Kantharia et al. 1998). CRRLs from the Galactic plane region have also been detected near 327 MHz (Roshi & Anantharamaiah 2000,2001a), near 76 MHz (Erickson et al. 1995), near 34.5 MHz (Kantharia & Anantharamaiah 2001) and near 26 MHz (private communication: S. Stepkin). Most of these have been confined to the inner Galaxy at longitudes less than 20° and arise in extended diffuse CII regions coincident with H I regions. CRRLs have thus been detected towards several directions in the Galactic plane, however the partially ionised gas towards Cas A remains the best studied region.

The sight line towards Cas A intercepts the Orion and Perseus arms of the Galaxy and the H I absorptions detected against Cas A are due to the cold neutral medium (CNM) in this direction. Much of the atomic hydrogen in the Galaxy has been observationally found to exist as 'warm' ($\sim 10^4$ K; warm neutral medium) and 'cold' ($\sim$ 70 K; CNM) gases. Models of the ISM indicate that these two temperature gases coexist in pressure equilibrium (Field, Goldsmith & Habing 1969) with a mean pressure, measured in the solar neighbourhood, of 2240 K cm^{-3} (Jenkins & Tripp 2001; see also Wolfire et al. 2003; Kulkarni & Heiles 1988, Dickey & Lockman 1990). The cold H I is observationally studied using 21cm absorption lines against background continuum sources (eg. Heiles & Troland 2003) as well as H I "self-absorption" (HISA; eg. Knapp 1974, Gibson et al. 2000, Kavars et al. 2005). HISA is due to H I absorption by cold atomic gas against bright background 21cm emission. While the temperature of cold gas is constrained by H I absorption studies (Heiles & Troland 2003), the gas pressure is measured using the ultraviolet absorption lines of CI (Jenkins & Tripp 2001). The cooling of the cold gas, which is predominantly due to C II (the most abundant gas phase ion in CNM) fine-structure transition, has been studied through observations of the 158 μm line emission (eg. Bock et al. 1993). Attempts have also been made to study the cold H I gas using the CRRL emission near 1.4 GHz (Crutcher 1977).

In this paper, we suggest, for the first time, the association of low frequency CRRL with the cold H I gas observed as HISA features in the Galactic plane. Stimulated emission due to the galactic background continuum radiation facilitates detection of CRRLs in emission near 327 MHz from this cold gas. We also, for the first time, suggest that the CRRLs detected from the Galactic centre direction arise in the Riegel-Crutcher (R-C) cloud (Riegel & Crutcher 1972), a prominent HISA. Although earlier studies have indicated that the carbon lines are formed in the same LSR velocity range over which H I absorption and ^{12}CO emission are observed in the inner Galaxy (Erickson, McConnell, Anantharamaiah 1995, Kantharia & Anantharamaiah 2001) the association of CRRLs with HISA in the inner Galaxy has not been discussed earlier. A summary of the 327 MHz recombination data is given in Section 2, which is followed by a discussion on the association of CRRL with cool atomic gas (Section 3). In Section 4 we focus on the R-C cloud, and demonstrate that CRRL and H I data can be combined to determine the physical properties of the line forming region. In Section 5 we use the estimated physical properties to investigate heating and cooling of the gas in the R-C cloud and molecule formation in the cloud. The results are summarised in Section 6.

2 SUMMARY OF OUR CRRL DATA

The ORT recombination line survey data were obtained with two angular resolutions ($2^\circ \times 2^\circ$; Roshi & Anantharamaiah 2000; $2^\circ \times 6'$; Roshi & Anantharamaiah 2001a). A galactic longitude range $-28^\circ < l < 89^\circ$ and latitude $b = 0^o$ was covered in the low resolution ($2^\circ \times 2^\circ$) survey. CRRLs have been detected almost contiguously from $-2^\circ < l < 20^\circ$ and also in a few positions at other longitudes (Paper I). A few of these positions were then 'mapped' with the high resolution beam ($2^\circ \times 6'$; Roshi & Anantharamaiah 2001a). In Paper I, we discussed some of the results from this survey. Summarising, we find that the radial distribution of the CRRLs near 327 MHz is similar to that of star-forming regions traced by the 3 cm hydrogen RRLs (Lockman 1989) and ^{12}CO (Dame et al. 1987). Our multi-resolution ORT data also indicate that some of the diffuse C II regions have an angular extent of a few degrees.

3 CRRLS AND H I SELF-ABSORPTION REGIONS

We use the median line width ($\sim$ 17 km s^{-1}) to classify the CRRLs detected in the ORT survey into two groups – (a) lines with width (FWHM) $\lesssim$ 17 km s^{-1} ("narrow lines") and (b) "broad lines" with width $\gtrsim$ 17 km s^{-1}. The median line width is obtained from the $2^o \times 2^o$ survey data. In Fig. 1, we show an example CRRL spectrum, obtained toward $l = 13^o.9$, $b = 0^o$. The spectrum shows broad ($\Delta V =$ 41.5 km s^{-1}) and narrow ($\Delta V = 6.8$ km s^{-1}) components. The broad lines detected toward G13.9+0.0 and other direction in the survey may consist of several narrow components as indicated by the higher angular resolution observations (see paper I). However, further high sensitivity, high angular resolution observations are needed to confirm this and hence we do not discuss the broad CRRLs any further. In this paper we focus on the origin of the narrow line emitting region. The parameters of the narrow line emission obtained from a Gaussian fit to the spectrum towards $l = 13^o.9$, $b = 0^o$ are given in Table 1. The H I spectrum toward the same direction obtained from the Leiden/Argentine/Bonn (LAB) survey (Kalberla et al. 2005, angular resolution $0^o.6 \times 0^o.6$) is shown in the middle panel of Fig. 1. The spectrum obtained after smoothing the LAB data to $\sim 2^o \times 2^o$ resolution is shown in the lowermost panels of Fig. 1. A HISA feature is seen at the same LSR (Local Standard of Rest) velocity as the narrow carbon line. The HISA is prominent in the higher resolution ($0^o.6 \times 0^o.6$) spectrum (see Fig. 1). The parameters of the HISA are included in Table 1. The coincidence of

Table 1. "Narrow" 327 MHz CRRL and H I line parameters

Source name	CRRL [1] T_L/T_C [2] $\times 10^{-3}$	CRRL [1] ΔV (km s^{-1})	CRRL [1] V_{LSR} (km s^{-1})	H I [1] T_L (K)	H I [1] ΔV (km s^{-1})	H I [1] V_{LSR} (km s^{-1})	Comment
G2.3+0.0	0.55(0.04)	16.1(1.3)	6.4(0.6)	48.5(1.5)	4.2(0.2)	6.5(0.1)	R-C cloud
G4.7+0.0	0.76(0.06)	8.5(0.07)	7.0(0.3)	64.7(2.3)	4.7(0.2)	7.0(0.1)	R-C cloud
G7.0+0.0	0.64(0.08)	12.1(1.9)	8.0(0.8)	51.0(1.5)	3.9(0.1)	7.1(0.1)	R-C cloud
G13.9+0.0	0.35(0.04) [3]	6.8(1.0)	18.4(0.4)	10.4(0.8)	5.3(0.5)	19.3(0.2)	
G18.4+0.0	0.36(0.05)	17.3(2.5)	24.1(1.1)	21.1(0.5) [4]	6.0(0.2)	22.8(0.1)	

[1] CRRL parameters for all positions except G13.9+0.0 are taken from Roshi & Anantharamaiah (2001b). The parameters for the position G13.9+0.0 are taken from Paper I. The CRRL data are obtained with an angular resolution of $\sim 2^o \times 2^o$. H I line parameters are obtained from Kalberla et al. (2005) after smoothing the data to an angular resolution of $\sim 2^o \times 2^o$.
[2] T_L/T_C is approximately the carbon line optical depth near 327 MHz. T_C is the background continuum temperature at the observed frequency.
[3] The given value is in T_L/T_{sys}, where T_{sys} is the system temperature.
[4] The HISA parameters are obtained from the $0^o.6 \times 0^o.6$ H I spectrum centred at $l = 18^o.5$ and $b = 0^o.0$.

the LSR velocities of the two lines implies that the two line forming regions coexist, if we make the standard assumption that the LSR velocities are due to galactic differential rotation; spectral traces having the same LSR velocities originate from regions at the same line-of-sight (LOS) distances. The widths of the two spectral lines, CRRL and H I line, differ with the CRRL being broader compared to H I line. The origin of this difference is discussed in Section 4.

Majority (63%) of the narrow CRRLs observed in the $2^o \times 2^o$ ORT survey have a corresponding HISA feature at the same LSR velocity. Absence of a corresponding HISA in some of the directions where narrow CRRLs are observed may be due to the following reason. Detection of HISA depends on favourable observing conditions. In order to detect a cool H I cloud in self-absorption, background H I emission with brightness temperature greater than the spin temperature of the cool cloud is required. Variation in the background emission temperature over the observing region can make the self-absorption difficult to detect, especially when observed with a coarse angular resolution. The need for higher angular resolution H I observations to detect HISA has been demonstrated, for example, by Bania & Lockman (1984). CRRLs do not need such favourable conditions for their detection. In Fig. 2 we show examples where narrow carbon lines are detected but no HISA is seen in the $2^o \times 2^o$ averaged H I spectrum (lowermost panels). While the higher angular resolution ($0.6^o \times 0.6^o$) H I spectrum (middle panel) shows an HISA feature towards G18.4+0.0, no such feature is seen toward G16.1+0.0 even in the higher angular resolution spectrum.

The H I spectra obtained close to the Galactic plane show a wealth of structures and many of these structures are self-absorption features as shown, for example, by Bania & Lockman (1984) in their high angular resolution observations. The ORT survey have not detected carbon lines corresponding to all these features. The typical upper limit on the CRRL optical depths from these features is $\sim 2.0 \times 10^{-4}$ (Roshi et al. 2002). The possible reasons for these are : (1) the CRRL survey is biased toward detecting carbon line emitting regions with large angular extent such that the beam dilution factor is insignificant; (2) the optical depth of CRRLs in all the regions are not high enough to detect them. Variation in carbon optical depth is seen, for example, towards the R-C cloud (see Section 4). (3) the Galactic non-thermal background radiation field is not strong enough to make the CRRL detection possible. The low Galactic radiation field may be the reason for non-detection of CRRLs toward HISA at $l \gtrsim 20^o$.

Difficulties in quantifying the observed properties of HISA features have been elaborated by several authors (eg. Levinson & Brown 1980). The observed line parameters listed in Table 1 are obtained by fitting a Gaussian to the absorption feature after removing 2nd or 3rd order polynomial "baseline" to the H I emission near this feature. Levinson & Brown (1980) have also shown, through simulation, that the observed central velocity of the H I absorption can be 'shifted' compared to the actual central velocity and this shift depends on the slope of the background H I emission. A rough estimate of this shift in the cases listed in Table 1 shows that it is insignificant compared to the errors in the line parameters.

A well known HISA feature towards the Galactic centre direction is the Riegel-Crutcher (R-C) cloud. In the next section, we concentrate on CRRL detection toward the R-C cloud. In particular, we demonstrate the usefulness of combining CRRL and H I observations to infer the physical properties and processes in the cloud. The physical processes that are discussed here are now part of well known numerical codes, which implement models for Photodissociation region (PDR; see for example Hollenbach & Tielens 1997, Hollenbach et al. 1991). Here we present a semi-analytic estimation of the physical properties and energetics in the R-C cloud. A detailed PDR modelling will be presented elsewhere.

4 THE RIEGEL-CRUTCHER CLOUD

A prominent cool neutral cloud (the R-C cloud; Riegel & Crutcher 1972, Heeschen 1955) has been observed in H I self-absorption in early surveys of the Galactic centre region. The self-absorption cloud has an extent of at least 40^o along the galactic longitude and $\sim 10^o$ along galactic latitude (Riegel & Crutcher 1972, Riegel & Jennings 1969). Line emissions from molecules such as ^{12}CO and OH have been detected

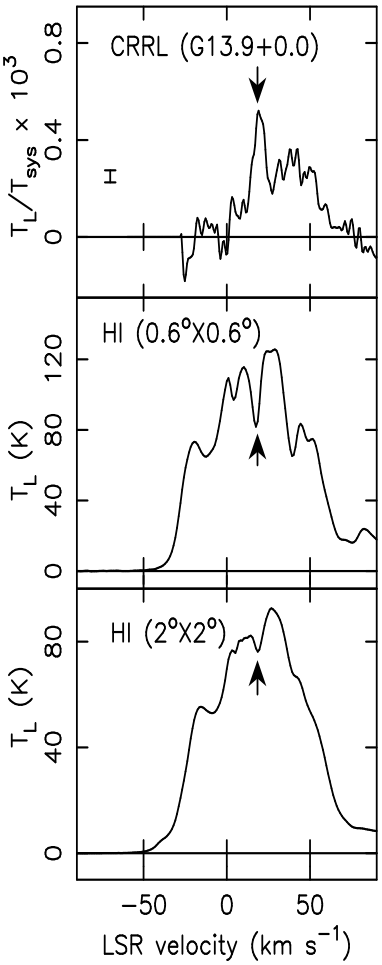

Figure 1. CRRL and H I spectra toward G13.9+0.0. CRRL (top panel) spectra at 327 MHz are obtained with an angular resolution of $2^o \times 2^o$. The 1σ value of the spectral noise is also shown in the top panel. The middle and bottom panels show H I spectra with angular resolutions $0^o.6 \times 0^o.6$ and $2^o \times 2^o$ respectively (Kalberla et al. 2005). The low resolution H I spectrum is centred at the galactic coordinates $l = 14^o.0$ and $b = 0^o$. The arrows are placed at the LSR velocity of the 'narrow' carbon lines. The good LSR velocity coincidence of 'narrow' CRRL and HISA features suggests an association between the two line forming regions.

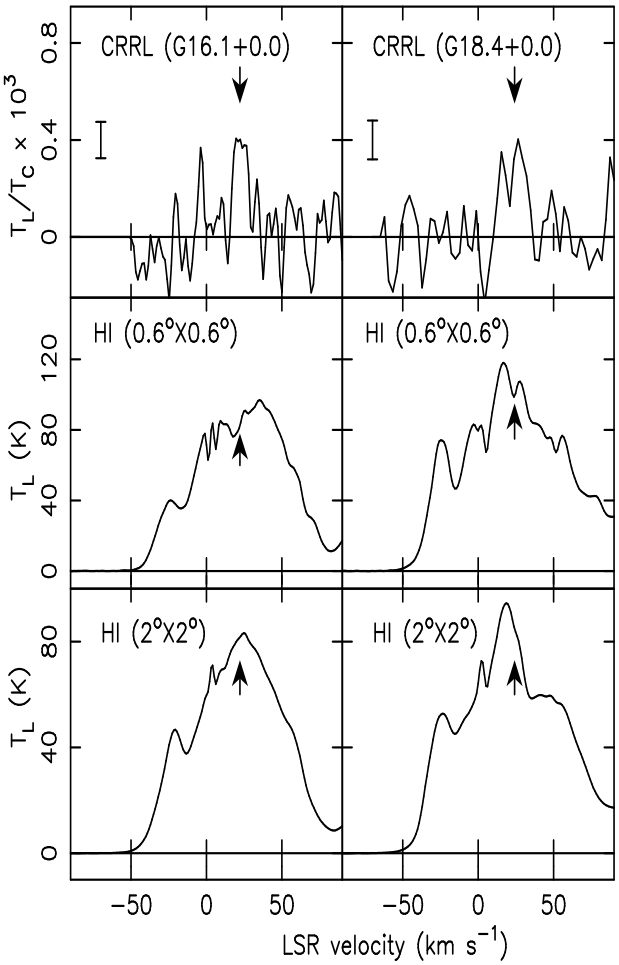

Figure 2. Examples of CRRL and H I spectra (Kalberla et al. 2005) toward G16.1+0.0 and G18.4+0.0 which show 'narrow' CRRL line (see top panels) emission but no HISA feature in the $2^o \times 2^o$ averaged H I spectra (bottom panels). CRRL (top panels) spectra at 327 MHz are obtained with an angular resolution of $2^o \times 2^o$. The 1σ values of the spectral noise are also shown in the top panels. The middle panels show H I spectra with angular resolutions $0^o.6 \times 0^o.6$. The low resolution H I spectra are centred at the galactic coordinates $l = 16^o.0$ and $18^o.5$ and $b = 0^o$. The arrows are placed at the LSR velocity of the carbon lines detected at the two positions.

in many directions toward the R-C cloud (Crutcher 1973). Distance to the R-C cloud was determined to be 125±25 pc from Na I observations against background stars (Crutcher & Lien 1984). Optical observations have also constrained the LOS thickness of the cloud to be between 1 and 5 pc (Crutcher & Riegel 1974). Recent high resolution ($\sim 100''$) H I line observations have revealed filamentary structures in the cloud with typical transverse width of 0.1 pc (McClure-Griffiths et al. 2006). McClure-Griffiths et al. (2006) also discussed the possibility that the LOS extent of the R-C cloud may be much smaller than 5 pc inferred by Crutcher & Riegel (1974) from their optical observations. They suggested that the LOS thickness may be ~ 0.1 pc, similar to the transverse width of the filaments. The H I absorption measurements have been used to infer a mean spin temperature of ~ 40 K and H I column density NH I of $\sim 10^{20}$ cm^{-2} for the R-C cloud (Montgomery, Bates, Davies 1995, McClure-Griffiths et al. 2006).

H I spectra toward the R-C cloud in the longitude range $\sim 2^o$ to 7^o are shown along with the CRRL spectra in Fig. 3. The angular resolution of H I spectra is $0^o.6 \times 0^o.6$ and that of CRRL spectra is 2^o (along b) $\times$ $0^o.5$ (along l). The prominent self-absorption feature seen in the H I spectra is due to the R-C Cloud. The H I line and CRRL parameters obtained from the spectra with 2^o (along b) $\times$ 2^o (along l) resolution in the same longitude range are given in Table 1. It is evident from Fig. 3 and the line parameters given in Table 1 that the LSR velocities of CRRLs and HISA coincide. Based on this coincidence we conclude that the carbon line forming regions are associated with the R-C cloud.

The R-C cloud extends from $\sim -15^\circ < l <\sim 25^\circ$ (Riegel & Crutcher 1972). However, CRRL emission from the R-C cloud could be identified only in the longitude range $\sim 2^o$ to 7^o. Close to the Galactic centre (ie $|l| \lesssim 2^o$) it is difficult to identify the CRRL emission associated with the

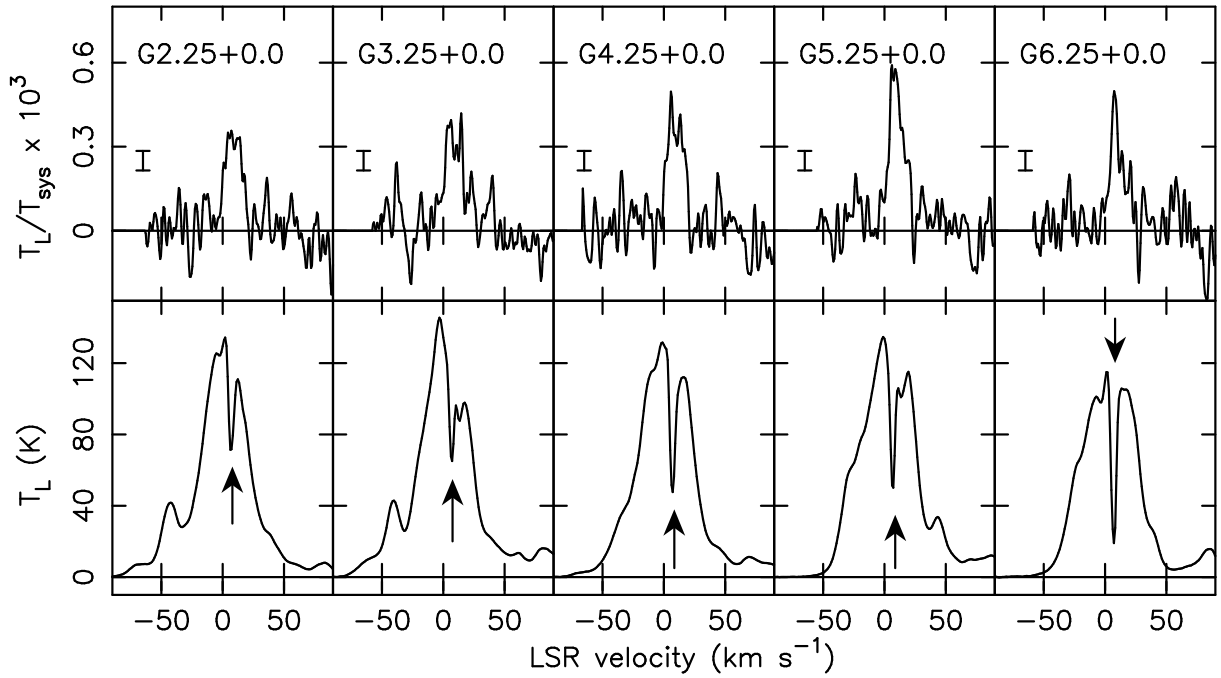

Figure 3. CRRL (top panels) and H I (bottom panels) spectra toward the Riegel-Crutcher cloud. CRRL spectra at 327 MHz and H I spectra (Kalberla et al. 2005) are obtained with angular resolution of 2^o (along b) × $0^o.5$ (along l) and $0^o.6 \times 0^o.6$ respectively The 1σ values of the noise in CRRL spectra are also shown in the top panels. The spectra are centred near the Galactic coordinates marked in the top panel. The arrows are placed at the LSR velocity of the carbon lines detected at the different positions.

R-C Cloud due to the degeneracy in LSR velocity of recombination line emission from several regions along the LOS. In other longitude range spanned by the R-C cloud the non-detection of CRRL emission may be either due to sensitivity limitation or due to variation in fraction of ionised carbon in the R-C cloud.

4.1 CRRL and HISA line widths

The average width of the carbon line from the R-C cloud is ∼ 12 km s^{-1} (FWHM) which is about 3 times the width of the H I absorption line (FWHM ∼ 4.0 km s^{-1}). CRRLs detected in several other directions also have a larger width compared to the H I line (see Table 1). If the two line forming regions coexist then the spectral lines from such regions are expected to have the same widths (this is true if the line widths are dominated by non-thermal motions, which is the case for the R-C cloud). A possible explanation for the difference in the line widths of CRRL and H I is the following. As mentioned above, detection of cool H I clouds in self-absorption needs favourable observing conditions and angular resolution (Bania & Lockman 1984). On the other hand, detection of CRRLs does not need such favourable conditions as long as the line forming regions fill a substantial portion of the observing beam and the Galactic background radiation field is strong. If there are several cool H I clouds with different velocities within the $2^o \times 2^o$ field of the CRRL observations, the coarser beam will detect a broad carbon line while the H I spectrum will be dominated by absorption due to the coldest gas. In addition, any velocity gradient within the observing beam can also contribute to the line width. Such a velocity gradient has been detected for H I absorption in the R-C cloud (Montgomery et al. 1995). The

Table 2. CRRL parameters observed toward the R-C Cloud

Freq (MHz)	CRRL [1]	$\int \tau_L d\nu$ [2] (s^{-1})	ΔV [2] (km s^{-1})	V_{LSR} [2] (km s^{-1})	Ref
327	C272α	9.2(1.4)	12.2(1.4)	7.1(0.6)	1
76	C441α	−3.9(0.7)	18.4(2.6)	5.5(1.3)	2
76	C555β	−3.3(0.6)	20.5(3.1)	2.2(1.6)	2
34.5	C575α	−1.9(0.3)	21.2(2.0)	10.2(1.4)	3

[1] Multiple transitions were observed at all three frequency bands. We list here the central transitions observed at each band.
[2] The 1σ errors on the line parameters are given in bracketed values

References: (1)Roshi & Anantharamaiah (2001b); (2) Erickson et al. (1995) ; (3) Kantharia & Anantharamaiah (2001)

R-C cloud also exhibits multiple H I absorption features (eg. Montgomery et al. 1995). Comparing CRRL and H I spectra obtained with similar (high) angular resolution can help in evaluating these possibilities.

4.2 Modelling the line forming region in the R-C cloud

The CRRL data toward the R-C cloud at 327 MHz combined with existing data at 76 MHz (angular resolution ∼ 4^o; Erickson et al. 1995) and 34.5 MHz (angular resolution ∼ $21' \times 25^o$; Kantharia & Anantharamaiah 2001) are used to model the physical properties of the line forming region. At 76 MHz both α and β transitions were detected toward the R-C cloud. To study the average properties of the C II region in the R-C cloud, all available CRRL data in the range $l \sim 2^o$

to $\sim 7^o$ and $b \pm 2^o$ at 327 and 76 MHz were averaged. These averaged values are listed in Table 2. Since the 34.5 MHz observations used a fan beam, no averaging was done and we have included the parameter fit to the spectrum towards $l = 5^\circ$ and $b = 0^\circ$. The line width and central velocities for all these transitions roughly match; any differences, particularly the difference between the 327 and 34.5 MHz line parameters, are attributed to the differences in the observing beam. To determine the physical properties, we followed the method described by Kantharia & Anantharamaiah (2001) where a uniform slab of line emitting region with electron temperature, T_e, electron density, n_e, and LOS extent, S, is considered.

The integrated line optical depth is related to these parameters through the equation (Shaver 1975)

$$\int \tau_L d\nu \approx 1.07\times10^7 \; b_n \; \beta_{n,\Delta n} \; K(\Delta n) \; \Delta n \; T_e^{-2.5} n_e^2 \; S \;\; \mathrm{s}^{-1}, \quad (1)$$

where b_n and $\beta_{n,\Delta n}$ are the non-LTE departure coefficients for principal quantum number n and transition Δn. K(Δn) = 0.1908 and 0.02633 for $\Delta n = 1$ and $\Delta n = 2$ transitions respectively. $\beta_{n,\Delta n}$ is defined as

$$\beta_{n,\Delta n} = 1 - 3.2 \times 10^{-6} \frac{n^3}{\Delta n} T_e \frac{b_n - b_{n+\Delta n}}{b_n}. \quad (2)$$

In the above equations the units of T_e is K, n_e is cm^{-3} and S is pc. The departure coefficients, which are computed using the programs of Payne et al. (1994), a modified version of the original program of Walmsley & Watson (1982), depend on the background continuum radiation field. We used 5000 K at 100 MHz as the background temperature. This background temperature is obtained from the continuum map at 34.5 MHz (Dwarakanath 1989; see also Kantharia & Anantharamaiah 2001) and scaled to 100 MHz using a spectral index of -2.6. The derived parameters of the line emitting region change by a few percent for a factor of 2 change in the background temperature. An abundance for carbon A_c of 1.4×10^{-4} obtained from the solar abundance of 2.9×10^{-4} (Lodders 2003) and assuming a depletion factor of 0.48 (Jenkins 2009, Wolfire et al. 2003) is used for the modelling. Since the R-C cloud has a large angular extent, no beam dilution factor is used for the 327 and 76 MHz observations to convert the observed line antenna temperature to brightness temperature. We could not find a single model which fitted all the three observed points. The 34.5 MHz observations were made with a beam $\sim 25^o$ in size along Galactic latitude and hence the observed line optical depth may have to be corrected by an unknown beam dilution factor. Therefore we constrained the model parameters using the 76 and 327 MHz data. Modelling of the data at 76 and 327 MHz resulted in the line forming regions having the following physical properties: $T_e \sim 40 \rightarrow 60$ K, $n_e \sim 0.8 \rightarrow 0.05$ cm^{-3} and $S \sim 0.03 \rightarrow 3.5$ pc. For T_e larger than 60 K we find that models with lower n_e ($\lesssim$0.05 cm^{-3}) also fit the CRRL data, however, the path lengths are longer than the LOS extent of 5 pc which is the thickness of the RC cloud as obtained by Crutcher & Riegel (1974). We, hence, rule out these higher temperature models.

The above modelling for the carbon lines used the departure coefficients estimated after including the dielectronic-like recombination process (Watson, Western & Christensen 1980, Walmsley & Watson 1982, see also Payne et al. 1994) which involves the excitation of the fine structure transition in the core electrons in carbon giving rise to a spectral line at 158μm. This process depends on the departure coefficients (RTE; Walmsley & Watson 1982) of the $2P_{3/2}$ and $2P_{1/2}$ states in carbon. RTE is obtained using statistical equilibrium for the $2P_{3/2}$ and $2P_{1/2}$ states. The equation of statistical equilibrium includes the density of colliding particles (electrons, H and H_2) which are estimated as described in Subsection 4.3, and iterated to get a consistent model. Table 3 gives three representative models consistent with the 327 and 76 MHz (both α and β transitions) CRRL observations. The expected integrated line optical depth as a function of quantum number for the three sets of model parameters listed in Table 3 are shown in Fig. 4. For each temperature listed in Table 3, the models are consistent with the data for a factor of 2 and 4 change in the listed densities and path lengths respectively.

4.3 Atomic and molecular hydrogen densities

We combine the CRRL and H I data to get more insight into the physical state of the R-C cloud. The inferred NH I for R-C cloud from H I observations is between a few times 10^{19} to 4×10^{20} cm^{-2}(Montgomery et al. 1995, McClure-Griffiths et al. 2006) which is typical of CNM clouds in our Galaxy. This high NH I implies that photoionisation due to EUV/soft X-ray does not dominate in the interior of the R-C cloud (see, for example, Glassgold and Langer 1974) and most of the ionisation is due to FUV photons which ionise carbon atoms. So, unlike in CNM clouds with canonical ISM pressure ($\sim$ 3000 K cm^{-3}), where electrons are due to ionisation of hydrogen atoms (Wolfire et al. 2003), most of the electrons in the R-C cloud are due to carbon ionisation. This fact can thus be used to estimate the number density of hydrogen, n_H, in the cloud; $n_H = n_e$ / A_c (see Table 3) where A_c is the number abundance of gas phase carbon atoms taken to be 1.4×10^{-4} (see Subsection 4.2). The fraction of hydrogen which is tied up in the atomic form, ie H I, is inferred as follows. The H I optical depth from the CRRL models is obtained by assuming that (a) some fraction of n_H is in atomic form (the remaining fraction is H_2 molecules) and (b) the spin temperature is equal to the electron temperature, which is generally the case for cold H I regions (eg. Kulkarni & Heiles 1988). In addition, we assume that the carbon and H I line forming regions co-exist along the LOS. This assumption means that, for models with $T_e \sim 60$ K and 50 K the LOS thickness of the H I region is respectively ~ 1.1 pc, close to the value suggested by Crutcher & Riegel (1974; ie 1 – 5 pc), and ~ 0.15 pc, close to the suggested value of 0.1 pc by McClure-Griffiths et al. (2006). For models with $T_e \sim 40$ K, the LOS thickness of the H I region will be 0.05 pc. For these models, it is possible that the CRRL emission originates from an interface region between the H I and H_2 in the R-C cloud. PDR modelling of the R-C cloud is needed to investigate this possibility. Following literature, we define the molecular fraction in terms of the n_{H_2} content; $f = \frac{2n_{H_2}}{n_{HI}+2n_{H_2}} = \frac{2n_{H_2}}{n_H}$, where n_{H_2} and n_{HI} are the H_2 and H I densities respectively. The H I optical depth due to CRRL models are then equated to the observed value (mean peak optical depth in the R-C cloud ~ 0.7; McClure-Griffiths et al. 2006) to determine f. The estimated f, n_{HI}, n_{H_2} and H I

Table 3. Physical properties of the Riegel-Crutcher cloud[a]

Model No.	T_e (K)	n_e (cm^{-3})	S (pc)	n_H (cm^{-3})	Av	n_{HI} (cm^{-3})	n_{H_2} (cm^{-3})	f	P_{HI} [1] ($\times 10^3$)	NH I (cm^{-2}) ($\times 10^{20}$)	NH_2 (cm^{-2}) ($\times 10^{20}$)
1	60	0.1	1.1	700	1.4	90	300	0.9	5	3	11
2	50	0.3	0.15	2100	0.6	500	800	0.8	27	2.5	3.7
3	40	0.6	0.04	4300	0.3	1430	1430	0.7	57	1.8	1.8

[a] T_e, n_e, S are the model parameters, n_H is the hydrogen nuclear density, Av is the visual extinction, n_{HI} is the hydrogen atomic density, n_{H_2} is the hydrogen molecular density, $f = 2n_{H_2}/n_H$ is the molecular fraction, NH I and NH_2 are the atomic and molecular column densities respectively.
[1] Partial pressure of H I is tabulated in units of K cm^{-3} .

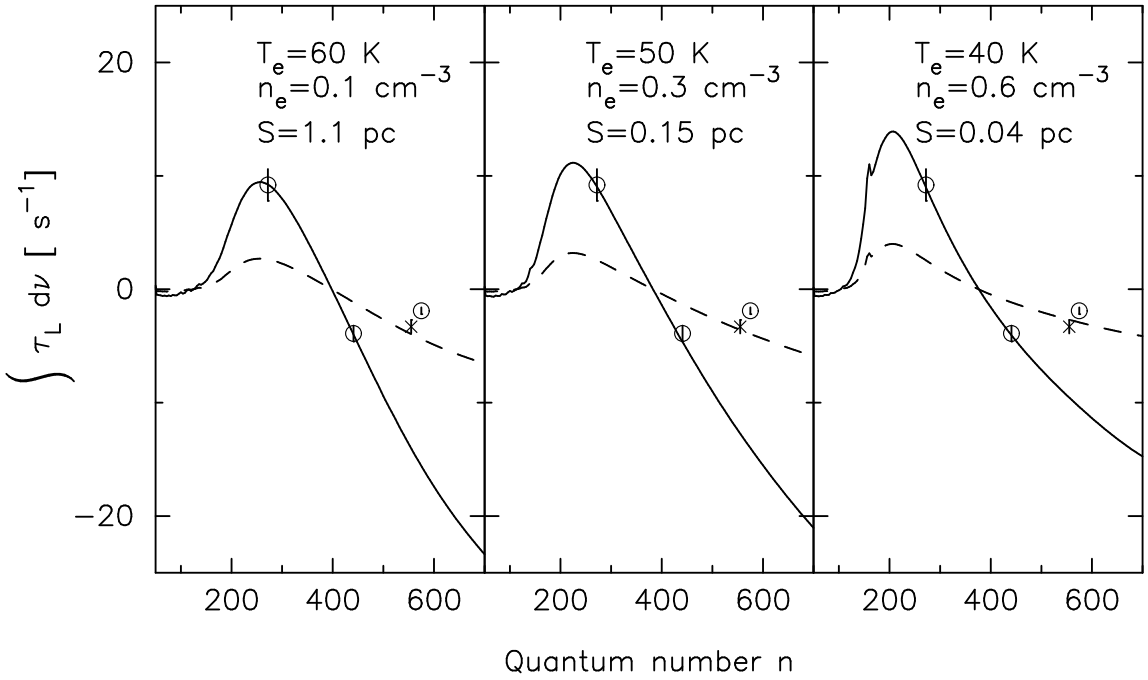

Figure 4. Integrated CRRL optical depth from models for the Riegel-Crutcher cloud plotted against principal quantum number. The optical depths of Cnα and Cnβ for the best fit model parameters are shown by solid and dashed lines respectively. The value of model parameters (electron temperature, T_e, electron density, n_e, and line-of-sight path length, S) are indicated on the plots. The observed integrated optical depths of Cnα lines are indicated by circles and that of Cnβ line is shown by cross. The error bars represent $\pm$ 1σ values.

partial pressure, $P_{HI} = n_{HI}T_e$ for the three representative models are listed in Table 3.

The higher temperature models (ie $T_e \sim 60$ K) have relatively low electron and H I densities. Their LOS extent is about a pc or more. The partial pressure of hydrogen is close to the mean interstellar pressure in the Solar neighbourhood. The molecular density compared to the H I density is higher in these models. The LOS extent of lower temperature models (ie $T_e \sim 40$ K) is ~ 0.05 pc. They have larger H I and electron densities. The molecular density is about the same as that of H I density. The H I partial pressure in these models is about an order of magnitude higher than the mean interstellar pressure. Note that for all the models the total gas pressure is at least an order of magnitude higher than the mean interstellar pressure and hence the cloud has to be supported by either gravity or magnetic pressure. In the next subsection, we compare the model predictions with other existing UV and optical observations with the intention of narrowing down the range of parameter values.

4.4 Comparison with UV and Optical observations

Several stars beyond the R-C cloud have been observed in the optical and UV, thus sampling the gas in the intervening cloud. From these observations we take data toward two stars, HD165246 (l=$6^o.4$, b=$-1^o.56$, distance=1.85 kpc; Jenkins 2009) & HD164402 (l=7^o,b=0^o, distance=1.74 kpc; Savage et al. 1977), which overlap with the directions in which CRRLs from the R-C cloud are observed. The measured visual extinction Av, towards these two stars are 1.1 and 0.95 and the measured NH_2 are 1.4 $\times 10^{20}$ cm^{-2} and 3 $\times 10^{19}$ cm^{-2}(Jenkins 2009, Savage et al. 1977) respectively. About 10% of the extinction and almost all the H_2 are due to the R-C cloud (Montgomery et al. 1995). Av from our

model parameters using the equation $\mathrm{Av} = \mathrm{NH}/(1.7 \times 10^{21})$ (Bohlin, Savage & Drake 1978) are listed in Table 3. The observed extinction due to the R-C cloud ie 0.11 to 0.095 is closest to our lower temperature ($T_e \sim 40$ K) model which predicts an extinction of 0.3 and NH_2 of 1.8×10^{20} cm^{-2}. Spectroscopic observations of the spectral lines of Na I (Crutcher & Riegel 1974), Mg I and Mg II (Bates, Montgomery, Kemp 1995) toward stars behind the R-C cloud can be used to determine the electron density in the cloud. The derived electron densities are typically < 0.1 cm^{-3} . Although we did find models with such low electron densities which fitted the observed data points, we do not favour these due to the long path-lengths, and hence correspondingly high Av, required to explain the observed line strengths. However, relaxing some of the assumptions made in deriving n_e from optical line observations can increase the estimated electron density. For example, Bates et al. (1995) obtained $n_e \sim 0.3$ cm^{-3} by considering that the Mg I line is mainly from the cloud core and the Mg II is distributed along the line of sight. This value is within the range of models that we derive for the carbon line forming region in the R-C cloud (see Table 3). However it is not sufficient to favour the lowest temperature model over the others. Thus, it appears that it is difficult to narrow down the range of physical parameters listed in Table 3 for the R-C cloud with existing data.

5 THE PHYSICAL STATE OF THE R-C CLOUD

In this section, we use the model parameters to investigate the cooling and heating processes in the R-C cloud. We also estimate the neutral carbon fraction and molecular formation and dissociation rates in the cloud.

5.1 Cooling in the R-C cloud

The derived properties of the R-C cloud are used to determine the cooling rate in the gas. The major cooling processes in these clouds are due to transitions in C II, C I and O I and molecular transitions in H_2 and CO. The C II 158 μm is believed to be the major coolant in diffuse clouds with temperatures ~ 100 K (Dalgarno & McCray 1972). The cooling rate due to C II 158 μm line emission is calculated following Watson (1984) and using the values for collision rate coefficients and Einstein A-coefficient given by Schöier et al. (2005). The combined cooling rate due to C I O I and molecular transitions in H_2 and CO is calculated from Fig 1. of Gilden (1984). These cooling rates along with the estimated intensity of the C II 158 μm line are given in Table 4 for the three representative models. The combined cooling rate due to atoms and molecules is at least a factor of 4 smaller than that due to the C II 158 μm emission.

5.2 Heating in the R-C cloud

The heating processes which are important in diffuse clouds and considered here are photoelectric emission, H_2 dissociation, carbon ionisation and cosmic rays. The heating efficiency of photoelectric emission depends on the grain charge which in turn is a function of the electron density and G0, the interstellar FUV (6 to 13.6 eV) radiation field in Habing unit (1.6×10^{-3} ergs sec^{-1} cm^{-2}; Habing 1968). The heating rate per unit volume due to photoelectric emission is given by (Wolfire et al. 2003)

$$\Gamma_{pe} = 1.3 \times 10^{-24}\ n_H\ \epsilon\ G0\ \ \mathrm{ergs\ s^{-1}\ cm^{-3}}, \tag{3}$$

where the photoelectric emission efficiency, ϵ is

$$\epsilon = \frac{4.9\times10^{-2}}{1+4\times10^{-3}(G0\ T_e^{0.5}/(n_e\phi_{PAH})^{0.73})} + \frac{3.7\times10^{-2}(T_e/10^4)^{0.7}}{1+2\times10^{-4}(G0\ T_e^{0.5}/n_e\phi_{PAH})}. \tag{4}$$

In the above equation, ϕ_{PAH} is a parameter introduced by Wolfire et al. (2003) to modify the electron-dust collision rates; following them we take its value to be 0.5. The values for n_e, n_H and T_e are taken from Table 3 for estimating the heating rate.

The second process we examine is fluorescent photodissociation of H_2. This process results in energetic H atoms which in turn lead to the heating of the cloud. The heating rate is essentially the product of the photodissociation rate per unit volume (see Eq. 7 in Subsection 5.4) and the mean kinetic energy (~ 0.25 eV) of the dissociated atoms (Stephens & Dalgarno 1973; Tielens 2005). We examine the relative importance of the four processes in heating the HISA cloud for G0 ranging from 1 to 10. We find that heating due to carbon ionisation (Tielens 2005) for a carbon neutral fraction $\lesssim 0.08$ (see Subsection 5.3) as well as cosmic ray heating are insignificant compared to the other two heating processes.

The photodissociation heating depends on the dissociation rate R_{phdiss}, which is a function of FUV radiation intensity inside the cloud. As described in Subsection 5.4, opacity of FUV lines in the cloud plays an important role in determining the dissociation rate inside the cloud. It can be shown that the opacity effect reduces the dissociation rate considerably at H_2 column densities $> 10^{14}$ cm^{-2}. This effect is termed 'self-shielding' (see for example Draine & Bertoldi 1996). Observations show that the H_2 column density of R-C cloud is $> 10^{19}$ cm^{-2}(Jenkins 2009, Savage et al. 1977). In clouds with such column densities detailed modelling shows that a gradient in the density ratio of hydrogen in atomic and molecular form exists and H_2 self-shielding becomes important (eg. van Dishoeck & Black 1986). Such detailed modelling, which are implemented in PDR codes (for example Hollenbach & Tielens 1997), are beyond the scope of the present work and will be presented elsewhere. In the subsequent part of the paper, we provide estimates of various quantities at a depth where the visual extinction (Av) is about half the total Av due to the cloud. We refer to this depth in the cloud as Av/2 and note that self-shielding effects need to be included while estimating the physical processes in the R-C cloud. Estimates of the heating at a depth of Av/2 for G0 ranging between 1 and 10 shows that photoelectric heating dominates in the cloud interior.

As mentioned above, photoelectric and photodissociation heating depends on the background FUV flux G0. Constraints on G0 may be obtained by assuming that the R-C cloud is in thermal equilibrium ie by equating C II 158 μm cooling rate per unit volume to the heating rate per unit volume. We estimate that G0 is between 4 and 7 (see Table 4). For comparison with photoelectric heating rate, which is approximately equal to the Λ_{CII} listed in Table 4,

Table 4. Thermal properties and H_2 formation/dissociation in the R-C cloud[a]

Model No.	Λ^1_{CII} ($\times10^{-23}$)	Λ^1_{other} ($\times10^{-23}$)	$\int I_{CII} d\nu$ [2] ($\times10^{-5}$)	G0	$\Gamma^{1,3}_{phdiss}$ ($\times10^{-25}$)	R_{form} ($\mathrm{cm^{-3}\ s^{-1}}$) ($\times10^{-11}$)	R^3_{diss} ($\mathrm{cm^{-3}\ s^{-1}}$) ($\times10^{-11}$)
1	12	3	3.3	4	0.1	0.2	0.003
2	74	8	2.7	7	5.6	2.4	0.14
3	153	14	1.5	6	28	11.6	0.7

[a] Λ_{CII} is the cooling rate due to C II 158 μm radiation, Λ_{other} is the total cooling rate due to atomic and molecular line emission, I_{CII} is the intensity of C II 158 μm line emission, G0 is the flux density of FUV radiation field in Habing unit, Γ_{phdiss} is the heating rate due to the dissociation of H_2 molecules, R_{form} and R_{diss} are the H_2 formation and dissociation rate respectively.
[1] The units of Λ_{CII}, Λ_{other} and Γ_{phdiss} are ergs $\mathrm{s^{-1}\ cm^{-3}}$
[2] The intensity of C II line is tabulate in units of ergs $\mathrm{s^{-1}\ cm^{-2} sr^{-1}}$
[3] Γ_{phdiss} and R_{diss} are estimated at Av/2. The Av obtained for the models is given in Table 3.

the heating rates due to photodissociation processes at Av/2 are included in Table 4 for the estimated G0.

5.3 Neutral carbon in the R-C cloud

In this section, we estimate the neutral fraction of carbon in the R-C cloud using our model parameters. To a large extent, the background FUV flux and the fraction of neutral carbon determines the ionisation of carbon in the cloud (see Glassgold & Langer 1975 for other factors affecting carbon ionisation). We estimate the neutral fraction by assuming that carbon ionisation is dominated by FUV radiation and that all electrons are due to carbon ions. The ionisation equilibrium of carbon implies

$$n_e n_{C^+} \alpha_R = f_C n_{C^+} \Gamma_{ion}, \tag{5}$$

where n_{C^+} is the number density of carbon ions, $\alpha_R = 6.38 \times 10^{-11}$ $\mathrm{cm^3\ s^{-1}}$ is the recombination coefficient (Nahar 1996) and $f_C = n_C/n_{C^+}$ is the neutral fraction. The ionisation rate, Γ_{ion}, is obtained by integrating the ionisation cross-section over the energy range 11.26 to 13.6 eV. For this integration, we used the radiation spectrum given by Draine (1978) and a constant ionisation cross section of 1.74 $\times10^{-17}$ $\mathrm{cm^2}$ (Nahar & Pradhan 1997). If we assume that the spectrum of the background radiation is independent of its integrated flux density i.e. G0, then Eq. 5 can be used to estimate f_C for the G0 required for thermal balance. The neutral fraction estimated at a depth of Av/2 is 0.08 for the model with $T_e = 60$ K and is 0.03 for the model with $T_e = 40$ K listed in Table 3. These are about a factor of 10 higher than the neutral fractions inferred for CNM clouds ($\lesssim 3\times10^{-3}$; Jenkins & Tripp 2001) but not unreasonable for clouds with H_2 column density $NH_2 \sim 10^{20}$ $\mathrm{cm^{-2}}$and G0 $\sim$ 5 (Hollenbach et al. 1991).

5.4 Formation and Dissociation of molecular hydrogen in the R-C cloud

The properties of the R-C cloud discussed above can be used to examine the formation and dissociation of H_2 in the cloud. Conventionally, the rate of formation of H_2 is obtained from the frequency of collision between H atoms and grains scaled by an efficiency factor for recombination on the grain surface. The collision rates depend upon the temperature and densities of H atoms and grains and the efficiency factor is estimated by making some reasonable assumptions regarding the properties of the grains (Hollenbach & Salpeter 1971). The rate of H_2 formation per unit volume can be written as (van Dishoeck & Black 1986)

$$R_{form} = 3 \times 10^{-18}\ T_e^{0.5}\ n_H\ n_{HI}\ y_{ef}\ \mathrm{s^{-1}\ cm^{-3}} \tag{6}$$

where y_{ef} is a parameter which takes into account the sticking probability and formation efficiency. y_{ef} is taken as unity for the calculations presented here. The formation rates obtained for the representative models vary from about 0.2×10^{-11} $\mathrm{s^{-1} cm^{-3}}$ for the highest temperature model to about 12×10^{-11} $\mathrm{s^{-1} cm^{-3}}$ for the lowest temperature model. These rates are given in Table 4.

The H_2 molecules in the cloud will be destroyed by FUV photons (11 to 13.6 eV) and cosmic rays. Photodissociation is initiated by line absorption (Lyman and Werner lines) and subsequent fluorescence to the vibrational continuum of the ground state of H_2 (P. M. Solomon 1965; private communication reported in Field, Somerville & Dressler 1966, Stecher and Williams 1967). Since the opacity to the UV lines from the H_2 molecule increases with depth (self-shielding) and several line transitions are involved, the dissociation rates at different depths are calculated numerically. Further, attenuation of FUV radiation field due to dust has to be taken into account to calculate the dissociation rate. An analytical approximation to the dissociation rate taking into account these effects is given by Draine & Bertoldi (1996);

$$R_{phdiss} = (NH_2/10^{14})^{-0.75} e^{-4.0Av} \times 4.17 \times 10^{-11}\ G0\ n_{H2}\ \mathrm{s^{-1}\ cm^{-3}}. \tag{7}$$

Here $e^{-4.0Av}$ takes into account the dust attenuation near $\sim$ 12 eV. The self-shielding effect is absorbed in the term $(NH_2/10^{14})^{-0.75}$, which is set to unity for $NH_2 \leqslant 10^{14}$ $\mathrm{cm^{-2}}$. We used the G0 estimated for thermal balance (see Table 4) to determine the dissociation rate per unit volume at a depth of Av/2 in the cloud. The estimated values for dissociation rate per unit volume (tabulated in Table 4) for the different models are more than an order of magnitude smaller than the formation rate. This difference in rates may indicate that the R-C cloud is in the process of molecular formation similar to, for example, the HISA cloud G28.17+0.05 (Minter et al. 2001).

We used the survey data of Dame et al. (1987) to investigate whether ^{12}CO line emission is associated with the R-C cloud. A ^{12}CO line feature of similar LSR velocity and width as that of the observed H I line toward the R-C cloud is present in some directions. However, this ^{12}CO line feature is not detected over the entire extent of the R-C cloud. This may support the fact the molecular formation in the R-C cloud is not complete. At the estimated rate of molecular formation in the R-C cloud, it should take $\gtrsim 10^5$ years for converting all the H I to H_2.

6 SUMMARY AND FUTURE OBSERVATIONS

In paper I, preliminary analysis of CRRL data obtained as part of a 327 MHz recombination line survey of the Galactic plane were presented. In this paper, we have for the first time, shown that the CRRL arising near the Galactic centre within $l \sim 10^\circ$ show excellent kinematic correlation with the HISA features from the Riegel-Crutcher cloud arguing for a common origin for the CRRL and HISA features. The R-C cloud is a HISA cloud located about 125 pc in the Galactic centre direction. Additionally, we have reported association of low frequency CRRL emission with a few other HISA clouds in the inner Galaxy.

We have also demonstrated that low frequency CRRL data at several frequencies along with H I observations can be used to constrain the physical properties of the cold H I regions. For the analysis presented here we made use of the CRRL observations at 327 and 76 MHz along with H I data to model the physical conditions in the R-C cloud. We find that models which fit the 76 MHz and 327 MHz data and are constrained by the LOS size of the R-C cloud are the following: $T_e \sim 40 \rightarrow 60$ K, $n_e \sim 0.8 \rightarrow 0.05$ cm^{-3} and $S \sim 0.03 \rightarrow 3.5$ pc. The derived physical properties were used to examine the heating and cooling processes in the R-C cloud. The dominant heating and cooling processes were found to be photoelectric emission and the C II 158 μm line emission respectively. The thermal balance between these two processes was used to constrain the diffuse FUV flux density on the cloud, which in Habing units (G0) ranges between ~ 4 and 7. Further, we investigated the H_2 formation and dissociation in the cloud and found that the formation rate per unit volume exceeds the dissociation rate per unit volume by at least an order of magnitude. Based on this imbalance in the formation and dissociation rate we conclude that the RC cloud is in the process of converting from H I to H_2 and will convert all its atomic hydrogen into the molecular form in a time scale $\gtrsim 10^5$ years.

The cold H I gas observed as HISA features are ubiquitous in the inner Galaxy and form an important part of the ISM. Our analysis shows that combining CRRL and H I data can give important insight into the nature of these cold gas.

We investigate the possibility of imaging the CRRL emission from H I self-absorbing clouds with upcoming Square Kilometre Array Pathfinders. The Murchison Widefield Array (MWA), Australian Square Kilometre Array Pathfinder (ASKAP) and the Karoo Array Telescope (MeerKAT) are considered for the investigation. Observing CRRL emission with the Long Wavelength Array (LWA) is discussed by Peters et al.(2010) and hence will not be discussed here. High angular resolution observation with the upcoming arrays will help, for example, resolve the 'line width problem' (see Section 4.1). The integration times required to image CRRL emission from the inner Galaxy with the different arrays are listed in Table 5. The carbon line temperature is computed using the optical depth of $T_e = 50$ K model given in Table 3. The peak line temperatures (T_L) obtained from this model for line width of 12.2 km s^{-1}(see Table 2) and galactic background temperature of 500 K at 327 MHz are listed in Table 5. This background temperature is an average value over the angular resolutions of the interferometric observation. The RMS brightness temperature (σ_{RMS}) in K for observations with the dual polarised interferometers is calculated using the equation

$$\sigma_{RMS} = \frac{T_{sys}}{A_{eff}\sqrt{4N_{base}N_{line}\Delta f\ t_{int}}} \frac{\lambda^2}{\theta_r^2} \quad (8)$$

where T_{sys} is the system temperature in K, A_{eff} is the effective area in m^2, N_{line} is the number of recombination lines that can be simultaneously observed, Δf is the frequency resolution in Hz corresponding to the line width of 12.2 km s^{-1}, t_{int} is the integration time in sec. N_{base} is the number of baselines with length $\frac{\lambda}{\theta_r}$, where θ_r is the angular resolution of the image and λ is the observing wavelength. In the above equation the unit of λ is meter. Integration times listed in Table 5 are for detecting CRRLs at 4σ level. The estimated values show that imaging CRRLs with the MWA is feasible.

7 ACKNOWLEDGEMENTS

Late Prof. K. R. Anantharamaiah first suggested that we conduct the recombination line survey near 327 MHz with the Ooty Radio Telescope. We are grateful to Anantha for his guidance and support, to which we owe much of the work we have accomplished in our careers. DAR thanks F. J. Lockman and D. S. Balser, NRAO, Green Bank, for the many stimulating discussions and helpful suggestions. DAR is thankful to NCRA for providing local hospitality while a part of the work on the paper was done. DAR also thanks Resmi Verma, a visiting student at RRI, for helping with obtaining the 2^o averaged H I spectra and Divya Oberoi, MIT, Haystack Observatory for providing the MWA configuration details. We thank the referee Naomi McClure-Griffiths for comments which have helped improve the paper and for suggesting to include feasibility of observing CRRLs with the SKA Pathfinders.

REFERENCES

Bania, T. M., Lockman, F. J., 1984, ApJS, 54, 513
Bates, B., Montgomery, A. S., Kemp, S. N., 1995, MNRAS, 277, 811
Blake D. H., Crutcher R. M., Watson, W. D., 1980, Nature, 287,707
Bock, J. J., et al., 1993, ApJ, 410, L115
Bohlin, R. C., Savage, B. D., Drake, J. F., 1978, ApJ, 224, 132
Booth, R. S, et al., 2010, `http://www.skatelescope.org/PDF/RFP_MeerKAT_v1.1.pdf`
Crutcher, R. M., 1973, ApJ, 185, 857
Crutcher, R. M., Riegel, K. W., 1974, ApJ, 188, 481

Table 5. Integration time for detecting CRRLs with SKA pathfinders

Telescope	Freq (MHz)	T_L (K)	θ_r ($'$)	N_{base}	Tsys[1] (K)	A_{eff} (m^2)	N_{line}	t_{int} (hrs)
MWA	95	−6.1	22	30794	500 + 4200	23	30	22
	200	1.1	10	30794	70 + 850	20	15	38
MeerKAT[2]	700	0.02	5	400× f_c	32 + 82	100	20	120/f_c
ASKAP[3]	750	0.02	5.6	49	50 + 58	90	10	1000

[1] $T_{sys} = T_{rec} + T_{sky}$, where T_{rec} is the receiver temperature and T_{sky} is the contribution from the galactic background emission.
[2]The MeerKAT antenna configuration details are taken from Booth et al. (2010). We have scaled N_{base} approximately for the new 64 antenna configuration of MeerKat. Since the scaling factor is not known well, we included a correction factor f_c to indicate how the integration time changes with f_c. The 20 recombination lines will span the frequency range ∼ 600 to 800 MHz.
[3]The ASKAP parameters are taken from Gupta et al.(2008). The 10 recombination lines will span the frequency range ∼ 700 to 800 MHz.

Crutcher, R. M., 1977, ApJ, 217, L109
Crutcher, R. M., Lien, D. J., 1984, Goddard Space Flight Center Local Interstellar Medium, 81, 117
Dame T. M., et al., 1987, ApJ, 322, 706
Dalgarno, A., McCray, R. A., 1972, ARA&A, 10, 375
Dickey, J. M., Lockman, F. J., 1990, ARA&A, 28, 215
Draine, B. T., 1978, ApJS, 36, 595
Draine, B. T., Bertoldi, F., 1996, ApJ, 468, 269
Dwarakanath, K. S., 1989, Ph.D Thesis, Indian Institute of Science, Bangalore.
Erickson W. C., McConnell D., Anantharamaiah K. R., 1995, ApJ, 454, 125
Ershov, A. A., et al., 1984, SvAL, 10, 348
Ershov, A. A., et al., 1987, SvAL, 13, 8
Field, G. B., Goldsmith, D. W., Habing, H. J., 1969, ApJ, 155, L149
Field, G. B., Somerville, W. B., Dressler, K., 1966, ARA&A, 4, 207
Gibson, S. J., et al., 2000, ApJ, 540, 851
Gilden D. L., 1984, ApJ, 283, 679
Glassgold A. E., Langer W. D., 1974, ApJ, 193, 73
Glassgold A. E., Langer W. D., 1975, ApJ, 197, 347
Gupta, N., et al. 2008, ASKAP memo no. 016
Habing, H. J., 1968, Bull. Astr. Inst. Netherlands, 19, 421
Heeschen D. S., 1955, ApJ, 121, 569
Heiles, C., Troland, T. H., 2003, ApJ, 586, 1067
Hollenbach, D., Salpeter, E. E., 1971, ApJ, 163, 155
Hollenbach, D., Takahashi, T., Tielens, A. G. G. M., 1991, ApJ, 377, 192
Hollenbach, D., Tielens, A. G. G. M., 1997, ARA&A, 35, 179
Jenkins, E. B., Tripp, T. M., 2001, ApJS, 137, 297
Jenkins, E. B., 2009, ApJ, 700, 1299
Kalberla, P. M. W., et al., 2005, A&A, 440, 775
Kantharia, N. G., Anantharamaiah, K. R., Payne, H. E., 1998, ApJ, 506, 758
Kantharia N. G., Anantharamaiah K. R., 2001, JAA, 22, 51
Kavars, D. M., et al., 2005, ApJ, 626, 887
Knapp, G. R., 1974, AJ, 79, 527
Konovalenko A. A., Sodin L. G., 1981, Nature, 294,135
Konovalenko A. A., 1984, SvAL, 10, 384
Konovalenko A. A., 1990, Radio Recombination Lines: 25 years of Investigation, Proceedings of IAU Colloq, 125, Eds M. A. Gordon & R. L. Sorochenko, Dordrecht:Kluwer, p175
Kulkarni. S. R., Heiles, C., 1988, Galactic & Extragalactic Radio Astronomy, Eds. G. L. Verschuur & K. I. Kellermann, Springer-Verlag, New York Inc., p95
Levinson F. H., Brown, R. L., 1980, ApJ, 242, 416
Lockman, F. J., 1989, ApJS, 71, 469
Lodders K., 2003, ApJ, 591, 1220
McClure-Griffiths N. M., et al., 2006, ApJ, 652, 1339
Minter, A. H., et al., 2001, ApJ, 555, 868
Montgomery A. S, Bates B., Davies R. D., 1995, MNRAS, 273, 449
Nahar, S. N., 1996, ApJS, 106, 213
Nahar, S. N., Pradhan, A. K., 1997, ApJS, 111, 339
Payne H. E., Anantharamaiah K. R., Erickson W. C, 1989, ApJ, 341, 890
Payne H. E., Anantharamaiah K. R., Erickson W. C., 1994, ApJ, 430, 690
Peters, W. M., et al., 2010, to appear in A&A
Riegel, K. W., Jennings, M. C.,1969, ApJ, 157, 563
Riegel, K. W., Crutcher, R. M., 1972, A&A, 18, 55
Roshi A. D., Anantharamaiah K. R., 2000, ApJ, 535, 231
Roshi A. D., Anantharamaiah K. R., 2001a, JAA, 22, 81
Roshi A. D., Anantharamaiah K. R., 2001b, ApJ, 557, 226
Roshi, A. D., Kantharia, N. G., Anantharamaiah, K. R., 2002, A&A, 391, 1097
Savage, B. D., Bohlin, R. C., Drake, J. F., Budich, W., 1977, 216, 291
Shaver, P. A., 1975, Pramana, 5, 1
Schöier, F. L., et al. , 2005, A&A, 432, 369
Sorochenko, R. L, Walmsley, C. M., 1991, A&AT, 1, 31
Stecher, T. P., Williams, D. A., 1967, ApJ, 149, L29
Stephens, T. L., Dalgarno, A., 1973, ApJ, 186, 165
Stepkin, S. V., Konovalenko, A. A., Kantharia, N. G., Udaya Shankar, N., 2007, MNRAS, 374, 852
Tielens, A. G. G. M., 2005, The Physics and Chemistry of the Interstellar Medium, Cambridge University Press, Cambridge, U.K
van Dishoeck, E. F., Black, J. H., 1986, ApJS, 62, 109
Walmsley, C. M., Watson, W. D., 1982, ApJ, 260, 317
Watson, W. D., Western, L. R., Christensen, R. B., 1980, ApJ, 240, 956
Watson, D. M, 1984, Galactic and extragalactic infrared spectroscopy, Proceedings of the Sixteenth ESLAB Symposium, Dordrecht, D. Reidel Publishing Co., p 195
Wolfire, M. G., et al., 2003, ApJ, 587, 278